Identifying the phyllosilicate minerals of hypogene ore deposits in lateritic saprolites using the near-IR spectroscopy second derivative methodology

Maximilien Mathian, Benoit Hebert, Fabien Baron, Sabine Petit, Jean-Luc Lescuyer, Renan Furic, Daniel Beaufort

Identifying the phyllosilicate minerals of hypogene ore deposits in lateritic saprolites using the near-IR spectroscopy second derivative methodology

Maximilien Mathian[a,b,*], Benoit Hebert[a], Fabien Baron[c], Sabine Petit[a], Jean-Luc Lescuyer[d], Renan Furic[d], Daniel Beaufort[a]

[a] *Université de Poitiers, CNRS UMR 7285 IC2MP, HydrASA Bât. B35, rue Michel Brunet, 86022 Poitiers Cedex, France*
[b] *Sorbonne Universités, UPMC Univ Paris 06, CNRS UMR 7590 IMPMC, 4 Place Jussieu, 75005 Paris, France*
[c] *Université de Nantes - CNRS UMR 6112 Laboratoire de Planétologie et Géodynamique (LPG), 2 rue de la Houssinière, 44322 Nantes, France*
[d] *LA MANCHA Services France, 4-14, rue d'Aguesseau, 75008 Paris, France*

ABSTRACT

Infrared field-based reflectance spectroscopy in the Visible - Near-Infrared - Short-wave Infrared (VIS-NIR-SWIR) domain is a useful tool in mining geology particularly efficient for investigating the clay mineralogy of alteration haloes around ore deposits. It is used as a routine technique for the basic identification, mapping and semi-quantification of clay mineral species. However, the use of this technique for prospecting in hypogene deposits at depth in intertropical areas is strongly limited because of the presence of a thick, kaolinite-rich lateritic cover. Due to the strong IR absorption of kaolinite and the overlapping of its IR bands with those of most of the phyllosilicates in the SWIR domain, the use of field based near-infrared spectroscopy does not permit efficient identification and mapping of the phyllosilicates inherited from hypogene alteration that persist in the saprolite of lateritic profiles.

In this paper, we propose a methodology to enhance the detection and semi-quantification of hypogene phyllosilicate minerals in kaolinite-rich lateritic saprolites using calibration curves. Those curves are built from the NIR spectra of binary admixtures of kaolinite or smectite with muscovite, Fe-Mg chlorite, clinochlore or talc in different known proportions.

For each admixture series, calibration curves were established, based on investigation of two regions of interest within the NIR domain (1350–1470 nm and 2080–2500 nm) using a field-based spectrometer. For each binary mixture series of phyllosilicates, the second derivative of the NIR spectra was used to enhance the detection of the diagnostic absorption bands of each type of phyllosilicate, and hence to optimize the calculation of the intensity ratios between the diagnostic bands of the phyllosilicate components as a function of their percentage in the mixture. In presence of large amounts of lateritic kaolinite, the detection limit of the major types of hypogene phyllosilicates has been found at ranges from 5 to 10 wt% of the total clay content using the second derivative of the NIR spectra acquired with a field-based spectrometer. Above these aforementioned limits of detection, the semi-quantitative data obtained by comparing the NIR reflectance spectra of natural samples with those of the calibration curves could permit to map hypogene alteration haloes directly from the lateritic saprolite.

Finally the described approach has been successfully tested on natural samples from the skarn deposits of the Ity gold mine (Ivory Coast).

1. Introduction

Field-based near-infrared (NIR) reflectance spectroscopy has been routinely used in mining geology for over 30 years. It is now a robust and low-cost method that allows automatic analysis of IR-sensitive minerals in the Visible - Near-Infrared - Short-wave Infrared (VIS-NIR-SWIR) length range of the electromagnetic spectrum (350–2500 nm/4000–28,600 cm^{-1}) at field scale.

This spectroscopic technique aids in mineral identification and enables to perform a semi-quantitative determination of the major IR-sensitive minerals that make up ore deposits and their associated alteration halos. The IR radiation reflected from the surface of a sample is characteristic of the IR-sensitive minerals (e.g., phyllosilicates, carbonates, phosphates, and sulfates) (Dill, 2016) that have wavelength positions and distinctive profiles that can be used for their identification.

Several articles have considered the use of VIS-NIR-SWIR spectroscopy for ore characterization (Ramanaidou and Wells, 2015; Dill, 2016), to map ore deposits through airborne or space-based hyperspectral methods (Thompson et al., 1999; Lisowiec et al., 2007) and for the identification of gangue minerals and alteration haloes during mining exploration (Hunt and Ashley, 1979; Pontual et al., 1997; Herrmann et al., 2001; Hauff, 2014). Because critical anion complexes, such as the hydroxyls (OH groups) in the lattices of phyllosilicates, are stimulated by selected vibrations in the VIS-NIR-SWIR range, this methodology is particularly efficient for investigating the alteration mineralogy zoning, which is quite diagnostic of the proximity to ore in hydrothermal deposits (Edwards and Atkinsons et al., 1986; Herrmann et al., 2001; Sun et al., 2001; Post and Crawford, 2014; Hauff, 2014; Dalm et al., 2017).

VIS-NIR-SWIR spectroscopy has been efficiently used to map mineral associations within alteration systems related to low- and high-sulfidation gold deposits, porphyries, kimberlites, skarns, IOCG (iron oxide copper gold) deposits and unconformity uranium deposits (Hauff, 2014). Unfortunately, the use of field-based NIR reflectance spectroscopy to obtain a detailed understanding of hypogene deposits and their alteration systems is still limited to core logging of deposits exposed in deep drill holes in countries with mid-latitude climatic conditions. The presence of a thick lateritic overburden precludes the identification of the residual hypogene phyllosilicates that can be identified in outcrops. Due to the abundance of supergene kaolinite (and smectite in a lesser degree) in lateritic profiles and the very high IR sensitivity of such clay minerals (Joussein et al., 2001), the identification of the contributions from the residual hypogene phyllosilicates using the VIS-NIR-SWIR spectra acquired from routine analysis is very difficult.

Moreover, in the case of mixtures of clay minerals in natural samples, the diagnostic NIR absorption bands commonly overlap. The positions of the diagnostic bands of kaolinite in the SWIR domain are very close to those of most phyllosilicates commonly observed in alteration halos surrounding hypogene deposits (e.g., micas, illite, chlorite, and talc, as well as others).

The aim of this study is to enhance the detection and identification of hypogene phyllosilicates in natural samples of lateritic saprolites based on detailed analysis of NIR spectra of controlled series of binary mixtures of kaolinite or smectite with muscovite, chlorite or talc within two specific wavelength ranges (1350–1470 and 2080–2500 nm, respectively). For each type of binary mixture series of phyllosilicates, the second derivative of NIR spectra was used to carefully determine the position of the diagnostic absorption bands of each type of phyllosilicate and hence to optimize the calculation of the intensity ratios between the diagnostic bands of the phyllosilicate components as a function of their percentage in the mixture. Semi-quantitative information could also be obtained from the resulting calibration curves.

A comparison of the detection limit obtained for talc, muscovite and different types of chlorite mixed with kaolinite or montmorillonite is presented as a function of the approach applied (routine vs. second derivative method), the type of spectrometer (laboratory-based vs. field-based spectrometers) and the investigated region of interest of the IR spectrum (1350 to 1470 vs 2080 to 2500 nm). The method has been successfully applied to natural samples of the lateritic saprolite that overlies the skarn gold deposit of Ity (Ivory Coast).

2. Sampling

2.1. Binary mixtures of phyllosilicates

The limits of detection for minerals vary between mineral mixtures. It is necessary to first build calibration files of percentage mixtures (Hauff, 2014). Binary mixtures of phyllosilicates were prepared and mixed with quartz (which is inactive in the IR regions of interest investigated) to simulate a wide range of natural saprolites. To carry out this task, strictly controlled amounts of clay minerals were mixed with the orthoquartzitic sand of Fontainebleau ($SiO_2 > 98\%$), which was first washed free of clay minerals using multiple washing and ultrasonic treatments.

Different types of clay references were considered. 1) Georgia kaolinite KGa-1 (Source Clay Repository of the Clay Minerals Society) and 2) Wyoming montmorillonite Swy-2 (Source Clay Repository of the Clay Minerals Society) were used as analogues to supergene phyllosilicates. 3) Muscovite (Brazil), 4) Mg chlorite (Luzenac, France), 5) Fe-Mg chlorite (Cauterets, France) and 6) talc (Luzenac, France) were used as analogues to hypogene phyllosilicates. In the following parts of this study, the Mg-chlorite will be referred as clinochlore, and the Fe-Mg chlorite will be referred to "chlorite".

This study focused on 5 series of binary mixtures composed of 400 mg of sand and 100 mg of reference clays. Each series included 15 samples corresponding to different ratios of hypogene phyllosilicates and supergene phyllosilicates (0/100, 2/98, 5/95, 10/90, 20/80, 30/70, 40/60, 50/50 and the reverse). Kaolinite-muscovite, kaolinite-talc, kaolinite-chlorite, smectite-chlorite and smectite-clinochlore mixtures were investigated in this study.

2.2. The natural samples of the Ity gold mine (Ivory Coast)

The Ity gold mine district is located in the southern portion of the Ivory Coast, approximately 500 km northwest of Abidjan and 100 km from the Sassandra fault (Béziat et al., 2016). The local geology has been determined by deep drilling performed by the SMI Company under the saprolite horizon. The gold deposit is located in a small remnant of the Birimian formation (Milesi et al., 1989; Leube et al., 1990; Feybesse and Milési, 1994; Hirdes et al., 1996; Lawrence et al., 2013a,b) that has been intruded by granodiorite and rhyolites (Fig. 1). During their emplacement, these intrusions developed skarn aureoles (Einaudi, 1982; Meinert et al., 2005), which are the primary causes of gold mineralisation (Béziat et al., 2016).

The entire mine area is constantly leached during the rainy season (up to 9 months) and deep laterite formations have replaced the basement rocks at depths of up to 130 m, including 50 to 120 m of saprolite (Béziat et al., 2016). Below the massive laterite cover, specific depth-related mineralogical variations have been identified in the saprolite as a function of the nature of the hypogene hydrothermal alteration observed at greater depths, in the unweathered skarn deposit (Mathian et al., 2015). Four main types of skarn-related mineral assemblages were identified, each of which is characterized by at least one specific type of hypogene phyllosilicate. 1) Muscovite occurs in intrusions and related volcano-sedimentary formations; 2) Fe-Mg chlorite occurs in the endoskarn; 3) clinochlore occurs at the endoskarn/exoskarn transition; and 4) talc occurs in the exoskarn.

In a previous study focused on the laterite saprolite (Mathian et al., 2015), twenty-two samples were investigated (Appendices 5 and 6). Those samples, called Ity 1 to Ity 21, were divided in three families: 1) the hypogene phyllosilicates dominant, with a clear XRD and IR signal of those minerals; 2) the supergene phyllosilicates dominant, without any XRD or IR signal of hypogene phyllosilicates; 3) the samples with a small amount of hypogene phyllosilicates, with low intensity peaks in XRD patterns and a very weak IR signal of those minerals (i.e. no specific diagnostic bands are visible). Eight samples of this last family have been chosen to test the limit of the second derivative methodology on natural samples. These samples were located in the saprolite and at the base of the lateritic profile that overlies the skarn deposit. They are all representative of a specific zone within the skarn system (specifically, the intrusive pluton, endoskarn, endoskarn/exoskarn transition, exoskarn, and unaltered host rocks). They were selected to be the proxy of samples coming from the saprolite basement (Ity 1, 9, 14 and 19) and from a higher part of the saprolite (Ity 4, 7, 12 and 20).

All samples were crushed and sieved to size of < 50 μm to avoid any preferential mineral orientation. They were also dried using a microwave oven at 850 W for 3 min to remove the water absorbed onto the sample material without any structural disturbance.
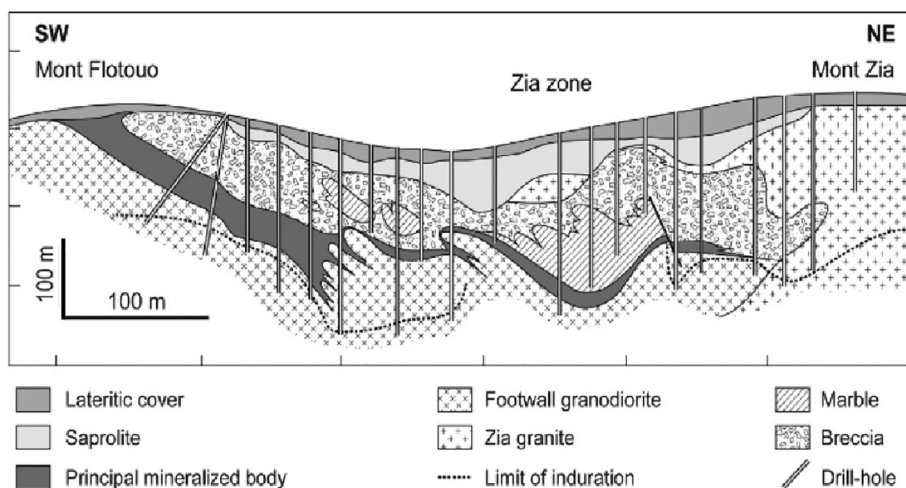
Fig. 1. Geological cross-section of the Ity gold mine deposits. (For interpretation of the references to colour in this figure legend, the reader is referred to the web version of this article.)
(Modified from Béziat et al., 2016.)

3. Methodology

Laboratory NIR spectra of natural and artificial binary samples were acquired directly from powders using a Thermo Scientific Integrating Sphere NIR with an internal InGaAs detector set on a Thermo Scientific Nicolet 6700 spectrometer equipped with a white light source and a CaF_2 beam splitter. Spectra were obtained by averaging 100 spectra with a resolution of 4 cm^{-1} in the 1000–2500 nm range.

Field VIS-NIR-SWIR spectra were acquired using an ASD TerraSpec 4® Standard-Res field-based spectrometer in the 350–2500 nm range. The spectral resolution was 3 nm in the 350–1000 nm range and 10 nm in the 1000–2500 nm range. Final spectra were obtained by averaging 50 spectra.

The second derivative procedure was employed to enhance the resolution of sharply defined features (which are hereafter named "components") where these overlap with broad bands. The components intensities were measured from the second derivative spectra from a baseline at Y = 0. The second derivative NIR spectra were obtained from the laboratory spectrometer using OMNIC™ software with a set of 13 points within the range of interest (number of points within the interval) and a polynomial function of order 3. For the field-based VIS-NIR-SWIR spectrometer, second derivative spectra were calculated automatically using The Spectral Geologist™ (TSG) software without modifiable parameters. Note that those parameters of calculation are not presented in the software or in the notice.

4. Results

4.1. NIR diagnostic bands of reference clay minerals

All phyllosilicate subtypes can be identified using diagnostics bands from two main domains of the NIR spectrum (Fig. 2) (Petit et al., 2004a; Madejova et al., 2011; Bishop et al., 2008). The first NIR domain contains wavelengths ranging from 2080 to 2500 nm (wavenumbers from 4800 to 4000 cm^{-1}). It includes mainly combination bands generated by combinations of OH stretching and OH bending or lattice vibration modes (Baron and Petit, 2016). The second domain contains wavelengths ranging from 1350 to 1470 nm (wavenumbers from 7400 to 6800 cm^{-1}). This spectral region contains mainly 2νOH bands, which represent the first harmonic of the OH stretching vibration subtype (Petit et al., 2004a). Hereafter, we present the characteristics of the diagnostic absorption bands of the different types of phyllosilicates investigated. The two domains will often be referred to as regions of interest (ROI).
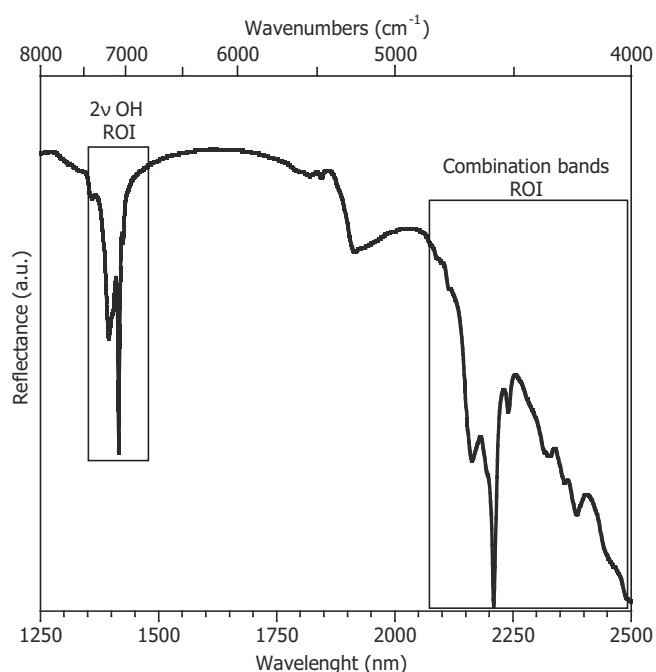

Fig. 2. The first region of interest (ROI) for phyllosilicates: $(\nu + \delta)$OH, from 2080 to 2500 nm, and the second ROI with 2νOH from 1350 to 1470 nm.

4.2. Kaolinite

Kaolinite is a 1:1 phyllosilicate and is the main supergene phyllosilicate resulting from lateritic alteration under tropical weathering conditions. The NIR spectrum of this mineral has 3 diagnostics bands in both of the regions of interest (Figs. 3a and 4a). In the 2νOH ROI, kaolinite is characterized by an intense band at 1415 nm (7065 cm^{-1}) and two other bands at 1406 and 1395 nm (7111 and 7169 cm^{-1}) that are attributed to $2\nu Al_2$OH vibration modes (Petit et al., 1999, 2004a). In the combination ROI of the NIR spectra, the three main diagnostic OH combination bands (Fig. 3a), which are located at 2210, 2194 and 2165 nm (4524, 4558 and 4627 cm^{-1}, respectively), yield very similar signals and are attributed to $(\nu + \delta)Al_2$OH vibration modes (Petit et al., 1999, 2004a).

4.3. Muscovite

White micas and illite are very common minerals in porphyry, skarn, epithermal and granite-related ore deposits worldwide (Cerny
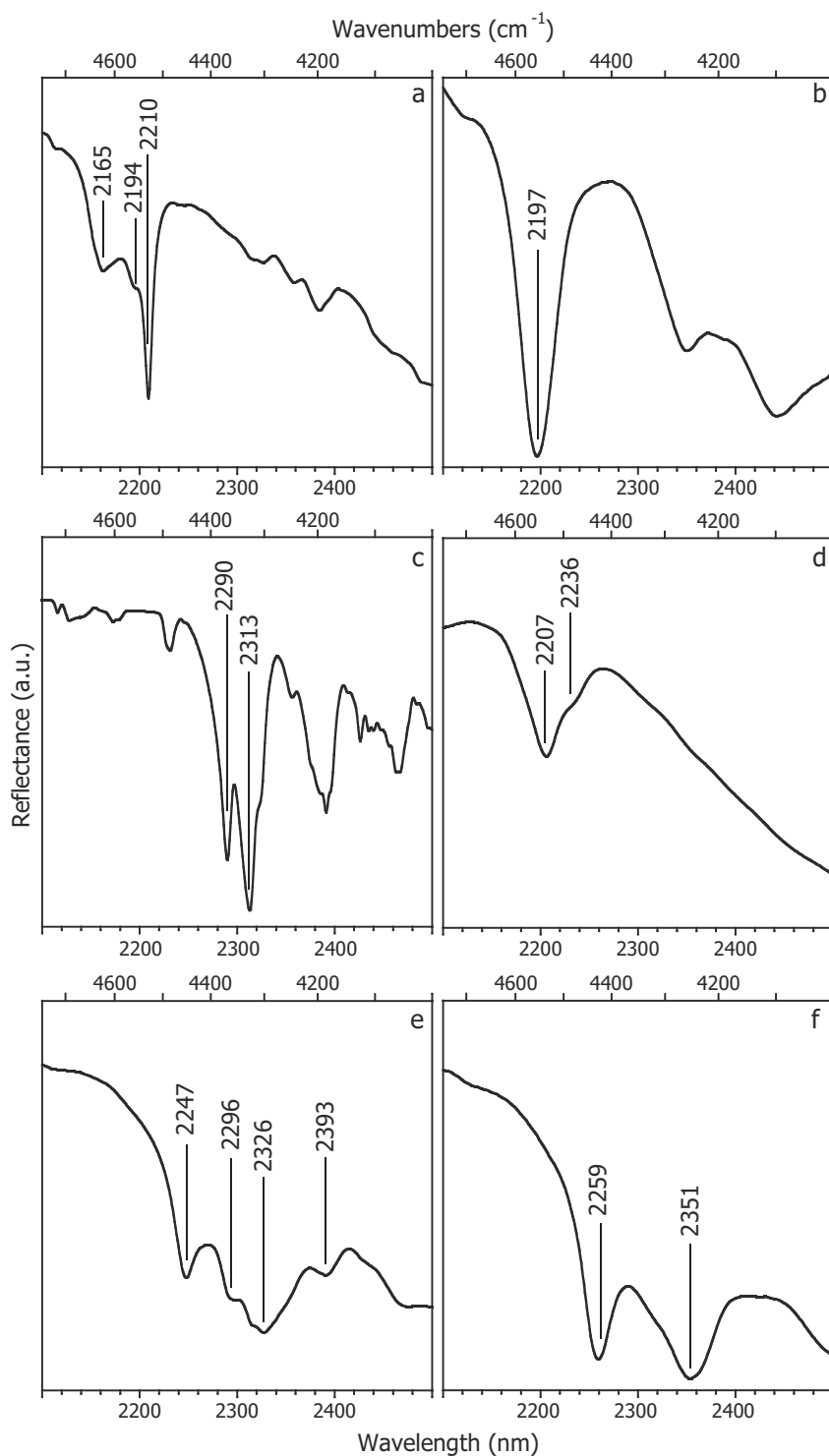
Fig. 3. Diagnostic bands of considered phyllosilicates in the first ROI (4800 to 4000 cm^{-1}). a: kaolinite, b: muscovite, c: talc, d: montmorillonite, e: clinochlore, f: Fe-Mg chlorite.

et al., 2005; Meinert et al., 2005; Seedorff et al., 2005; Simmons et al., 2005); Cerny et al., 2005). Muscovite and illite present very similar infrared spectra (Vaculikova and Plevova, 2005), which are characterized by two main intense diagnostic bands (Figs. 3b and 4b) that are located at 1412 nm (7083 cm^{-1}) and 2197 nm (4552 cm^{-1}). These bands are attributed to $2\nu Al_2OH$ and $(\nu + \delta)Al_2OH$ respectively (Post and Noble, 1993; Madejova et al., 2011).

4.4. Talc

Talc is a 2:1 non-swelling phyllosilicate rich in Mg. The NIR spectrum of talc is characterized by four intense bands (Figs. 3c and 4c). In the second ROI, the band located at 1391 nm (7186 cm^{-1}) is very sharp and is attributed to $2\nu Mg_3OH$ vibrations. The second band appears at 1398 nm (7152 cm^{-1}) and is attributed to $2\nu Mg_2Fe^{2+}OH$ vibrations (Petit et al., 2004a,b). In the combination ROI (Fig. 3c), the two bands related to talc are located at 2290 and 2313 nm (4366 and 4324 cm^{-1}). The precise explanation of their positions, which are due to stretching and bending combination bands, is not fully understood (Petit et al., 2004b; Madejova et al., 2011).
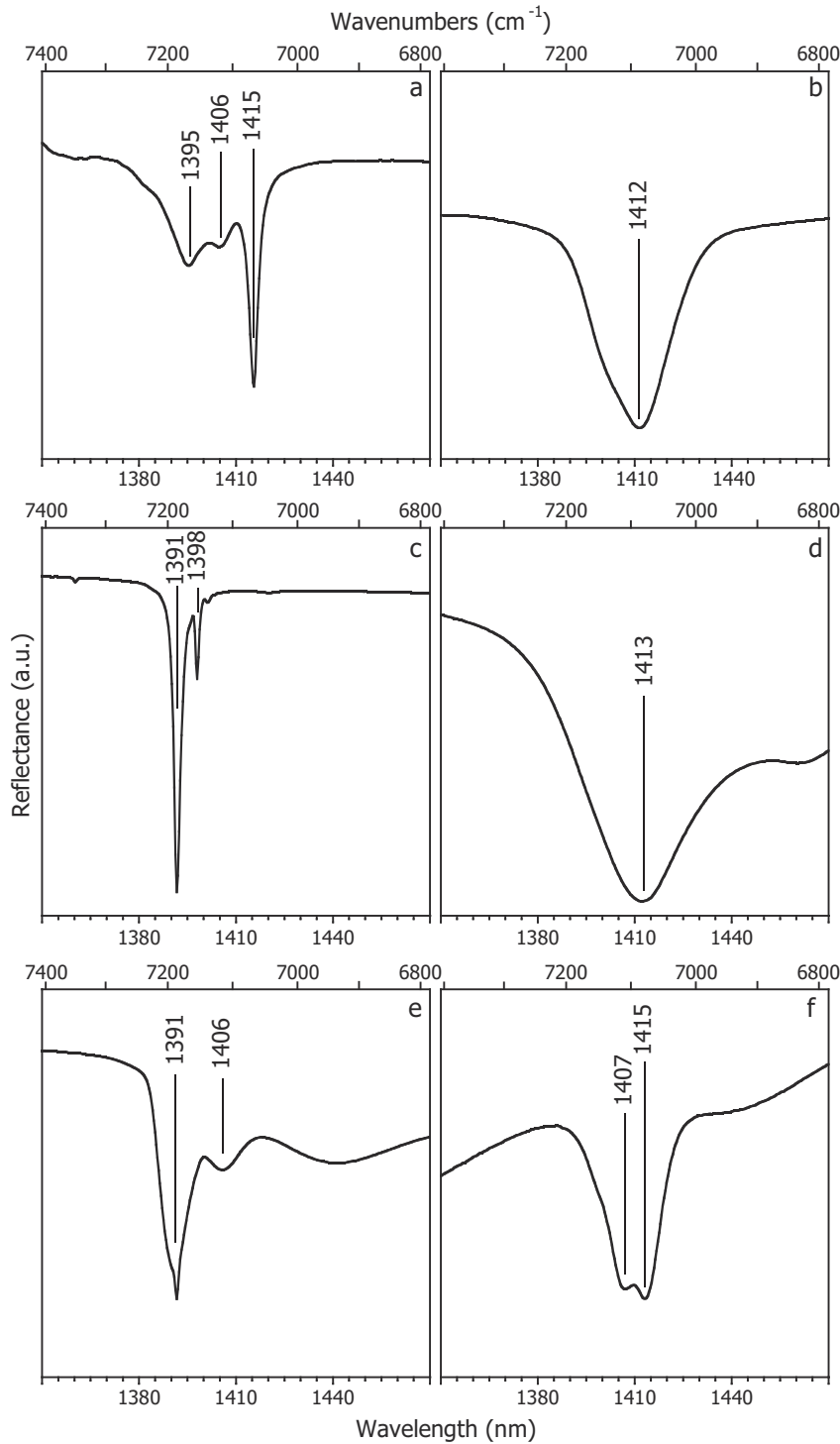
Fig. 4. Diagnostic bands of considered phyllosilicates in the second ROI (7400 to 6800 cm^{-1}). a: kaolinite, b: muscovite, c: talc, d: montmorillonite, e: clinochlore, f: Fe-Mg chlorite.
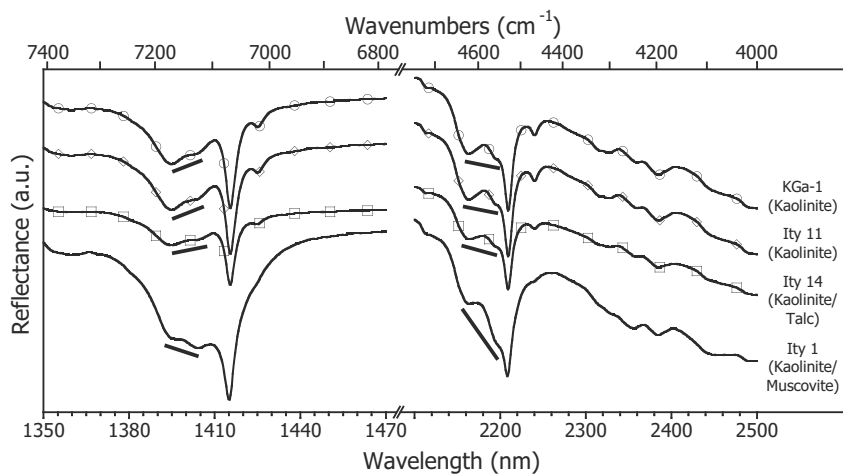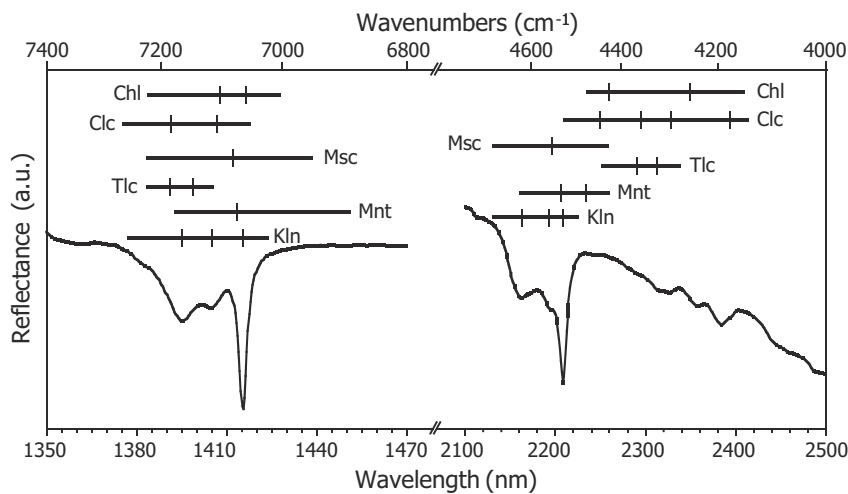
4.5. Montmorillonite

Montmorillonite is a 2:1 swelling clay mineral that is common near the bottom of lateritic profiles. In the combination region, two bands located at 2207 and 2236 nm (4529 and 4472 cm^{-1}) could be used as diagnostic bands to assess the presence of this smectite-type mineral (Fig. 3d). They are due to $(\nu + \delta)Al_2OH$ and $(\nu + \delta)AlFe^{3+}$ OH vibrations, respectively (Post and Noble, 1993; Petit et al., 2004a; Bishop et al., 2008; Madejova et al., 2011). It can also be easily recognized as a broad, complex band in the $2\nu OH$ region (Madejova et al., 2011) at 1413 nm (7077 cm^{-1}) that corresponds to $2\nu Al_2$-OH vibrations and to

the first overtone of water molecules involved in weak hydrogen bonding (Fig. 4d).

4.6. Chlorites

Clinochlore (Figs. 3e and 4e) and Fe-Mg chlorite (Figs. 3f and 4f) have distinctive diagnostic bands. The 1407 and 1415 nm (7106 and 7067 cm^{-1}) bands are characteristic of Fe-Mg chlorite in the second ROI. The Fe-Mg chlorite combination bands in the first ROI are well defined at 2259 and 2351 nm (4426 and 4253 cm^{-1}). The later chlorite bands have not been explained by a precise OH vibration signals

Fig. 5. Position and overlapping possibilities of the considered clay mineral diagnostic bands in the first and second ROI. Kaolinite and muscovite are overlapping in both regions as well as clinochlore and chlorite with montmorillonite. Talc only overlaps with kaolinite in the second ROI.

Fig. 6. IR spectra of kaolinite reference (KGa-2) and 3 natural samples rich in phyllosilicates: Ity 1 (kaolinite and muscovite), Ity 11 (kaolinite) and Ity 14 (kaolinite talc) in both ROI. Only kaolinite bands are visible, but the intensity of Ity 1 and 14 bands are different from those of the KGa-2 reference and Ity 11. Slope changes are visible on the kaolinite spectra under the influence of overlapped hidden bands of talc or muscovite.

(Madejova et al., 2011). In the second ROI, clinochlore has a broad band at 1391 nm (7185 cm^{-1}) that corresponds to $2\nu Mg_3OH$ vibrations, similar to the one observed in talc spectra (Ferrage et al., 2003). Clinochlore shows another band at 1406 nm (7111 cm^{-1}) that is not described in literature. In the first ROI, the diagnostic bands for clinochlore overlap. Four main combination bands could be identified for this mineral at 2247, 2296, 2326 and 2393 nm (4450, 4356, 4299, and 4179 cm^{-1}).

4.7. Identification of index absorption bands from NIR spectra of phyllosilicate mixtures

Supergene clay minerals (kaolinite and smectite) often constitute > 50% of the modal compositions of saprolites. They strongly absorb in the NIR domain, making the identification of the contribution of small percentages of hypogene phyllosilicates very difficult. However, even if the NIR bands of these phyllosilicates have very similar positions and hence overlap strongly, the difference in their intensity of IR absorbance at each wavelength results in additional shoulders in the IR spectrum when compared to the spectra of a reference kaolinite (KGa1) and a reference smectite (Swy2). Consequently, the occurrence of shoulders and changes in the IR bands profiles observed in the NIR spectra (Fig. 5) can be attributed to the contributions from the other phyllosilicate minerals present in the mixture. The presence of small amounts of talc and muscovite induced a change in the profiles of IR bands indicative of kaolinite (Fig. 6) with 1) a band apparition (1391/2290 cm^{-1}) and/or 2) an inversion of the

slope of kaolinite bands. This phenomenon was observed in both ROIs (1350–1470 nm and 2080–2500 nm) and is due to the increasing influence of the hidden bands of talc and muscovite. The presence of minor amount of chlorite in smectite-rich samples induced slight changes in both the shape and width of the main smectite band (Fig. 7). Such changes in the NIR profiles are, however, very weak.

All of the binary mixtures have been analyzed using both field-based and laboratory infrared spectrometers. Some variations were observed in NIR spectrum profiles as a function of the increasing percentages of hypogene phyllosilicates in the mixture. It was then possible to determine the detection limits of these minerals in kaolinite-rich and smectite-rich mixtures (Appendices 1, 2, 3 and 4).

For each series of binary mixtures, a visual limit of detection has been determined as the minimal percentage at which the hypogene phyllosilicate can be identified in the NIR spectrum from the occurrence of new bands or the evident modification of band profiles, without any spectral processing.

For kaolinite-rich admixtures, muscovite, talc and chlorite were detected visually in the NIR spectra when their percentages exceeded 40%, 10% and 40%, respectively. For smectite-rich admixtures, Fe-Mg chlorite and clinochlore were detected when their percentages exceeded 50% and 20%. Table 2 presents all the established visual limits of detection for both spectrometers and both regions of interest for each binary mixture series.
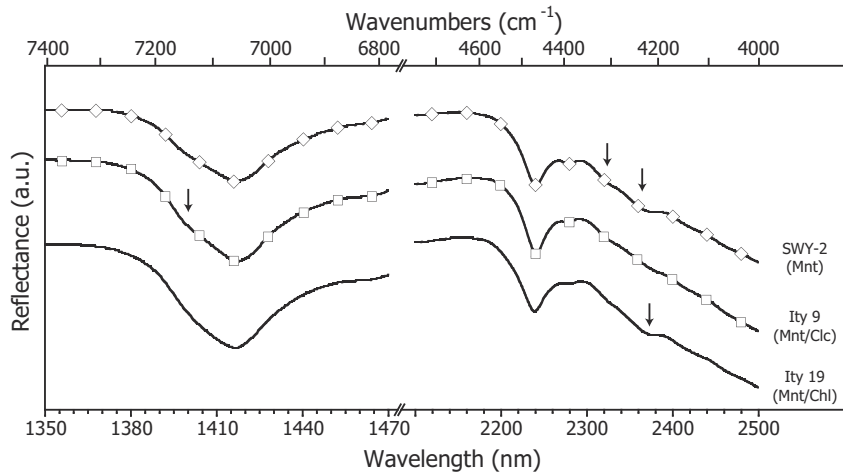
Fig. 7. IR spectra of montmorillonite reference (Swy-2) and 2 natural samples rich in phyllosilicates: Ity 9 (clinochlore and montmorillonite), Ity 19 (clinochlore and montmorillonite) in both ROI. Only smectite bands are visible, but IR spectra slope changes are visible in both natural samples traducing the presence of both chlorite types.

4.8. Improving the identification of hypogene phyllosilicates by using the second derivative curve of the spectra

The presence of minor amounts of phyllosilicates phases in natural samples cannot be easily detected because it consists only in subtle differences (i.e. inflection points) in the NIR reflectance spectra. However slight changes in the profile of the reflectance spectra can be highlighted by use of an algorithm that permit to calculate the second derivative curve. The second derivative curves of NIR spectra are especially useful for separating peaks of overlapping bands and are a good noise filter since changes in base line have negligible effect on derivatives. Every maximum (or minimum) observed in second derivative curve corresponds to an inflection point of the original reflectance spectrum and the components oriented upwards in the second derivative curves correspond to inflection points at a particular wavelength position of absorption bands. The fact that the intensity of the second derivative components is proportional to the intensity and width of their related IR bands in the reflectance spectrum (Fig. 8) makes it suitable for a semi-quantitative approach.

The derivation processes of the reflectance IR spectra were made using the software and parameters described in the corresponding methodology section. This procedure improved the detection limit of hypogene phyllosilicates. Fig. 8a and b show reflectance spectra for a kaolinite (50%) – muscovite (50%) binary admixture obtained from both field-based and laboratory spectrometers within the two regions of interest. The resolution of the NIR profiles obtained using the field-based spectrometer is lower than that of the NIR profiles from the laboratory spectrometer, particularly in the region between 1350 and 1470 nm (7400 to 6800 cm^{-1}). Fig. 8c and d show the second derivative curve calculated from the previous reflectance spectra.

The use of the second derivative overcomes the lower resolution of the field-based NIR spectrometer and makes it as reliable as the
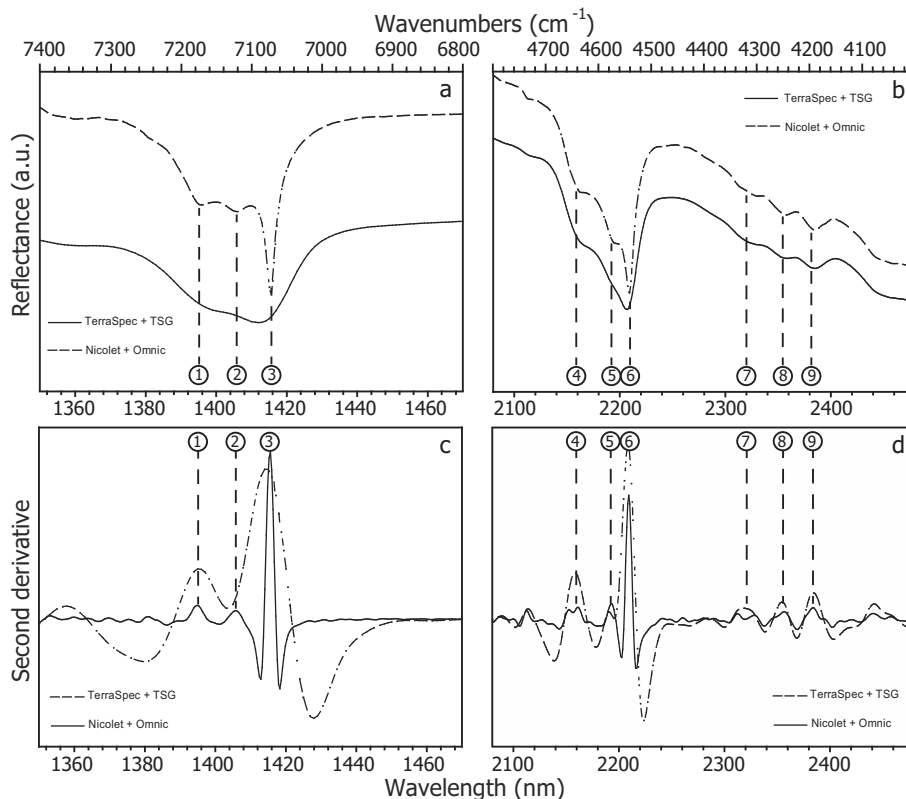

Fig. 8. Reflectance (a and b) and second derivative (c and d) spectra for a 50–50 kaolinite-muscovite binary admixture in both regions of interest using the laboratory and the field spectrometer.
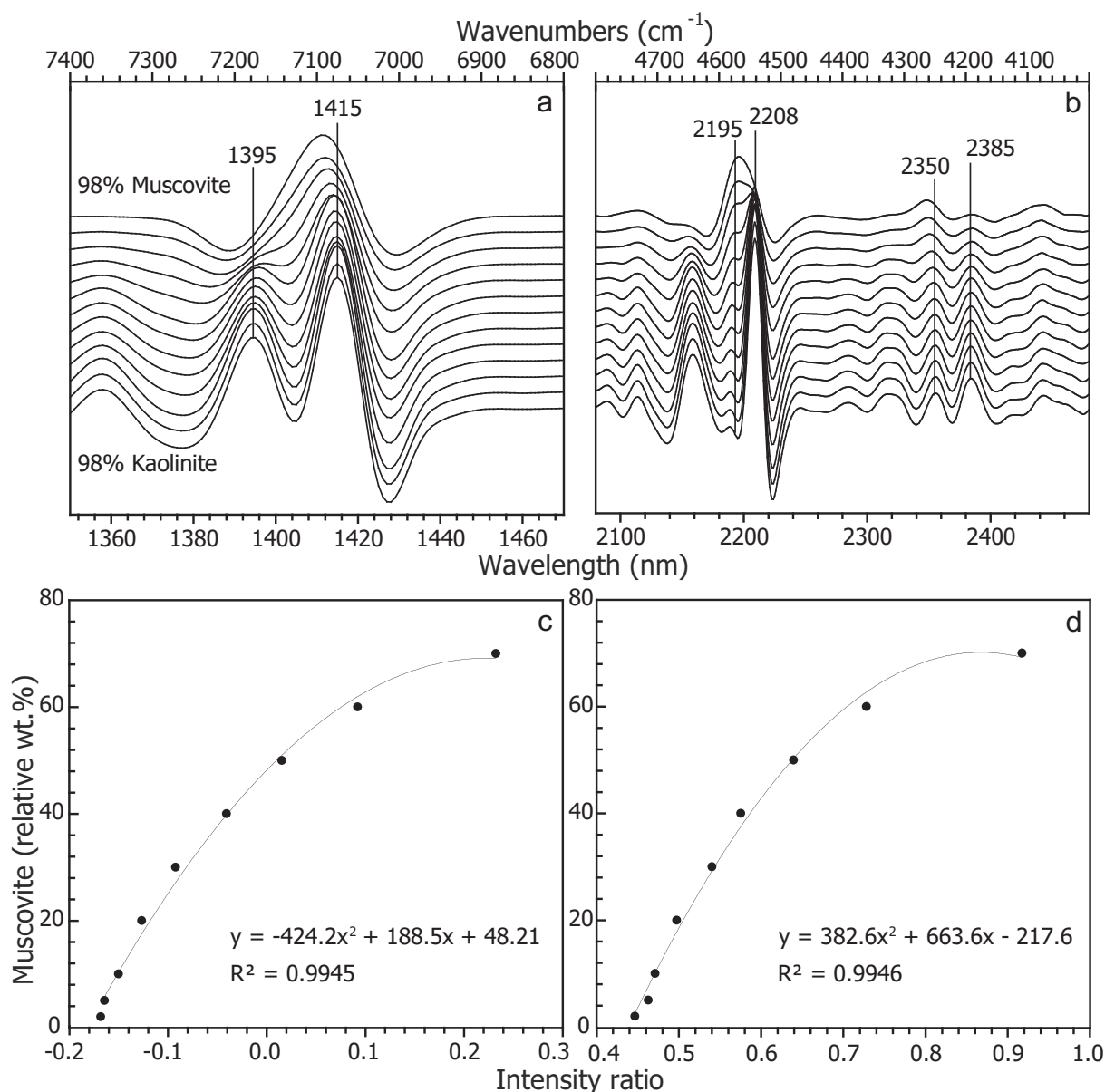
Fig. 9. Second derivative spectra (a and b) and calibration curves (c and d) of the muscovite-kaolinite binary admixture series. Reflectance spectra were acquired with the field spectrometer and derived using TSG.

laboratory spectrometer for the identification of band. The use of second derivative spectra allowed accurate measurement of intensity ratios between components whose positions fit with those of the index NIR bands of the phyllosilicates of interest. The aim of this work was to be able to provide a method that could be applied directly on the field, we will consider hereafter only the spectra obtained from the field-based spectrometer.

This section focuses on the detection limit of each type of hypogene phyllosilicate disseminated in a kaolinite or smectite matrix using the second derivative profiles of the binary admixtures. In the following figures, the spectra were offset for clarity, and an error of $\pm$ 5 nm and $\pm$ 10 cm^{-1} has been assumed for the IR band positions.

4.9. Kaolinite–muscovite mixtures

The second ROI (Fig. 9a) was not found useful for identification of low relative amounts of muscovite; as it allowed the identification of

this mineral only when its percentage exceeds 70 wt% of the phyllosilicate content in the mixture.

In the first ROI (Fig. 9b), the presence of muscovite was indicated by two components at 2195 and 2350 nm. Here, kaolinite showed four main components at 2165, 2208, 2360 and 2385 nm. The qualitative parameter for the detection of muscovite in a kaolinite-rich sample was calculated following the ratio of intensities (called "$I_{component\ position\ 1}/I_{component\ position\ 2}$" and measured as explained in the methodology section) between the muscovite component at 2195 nm and the kaolinite component at 2208 nm given by I_{2195}/I_{2208}. The calibration curve, i.e. the correlation between the intensity ratio and the amount of the considered phyllosilicate compared to the total mass of phyllosilicates in the admixture, was obtained from a least square polynomial regression (Fig. 9c). Only one fitting method was used in this study but improvements could be obtained after testing other methods on these datasets. It is important to remind that these calibration curves are mathematical proxies to describe the second derivative components
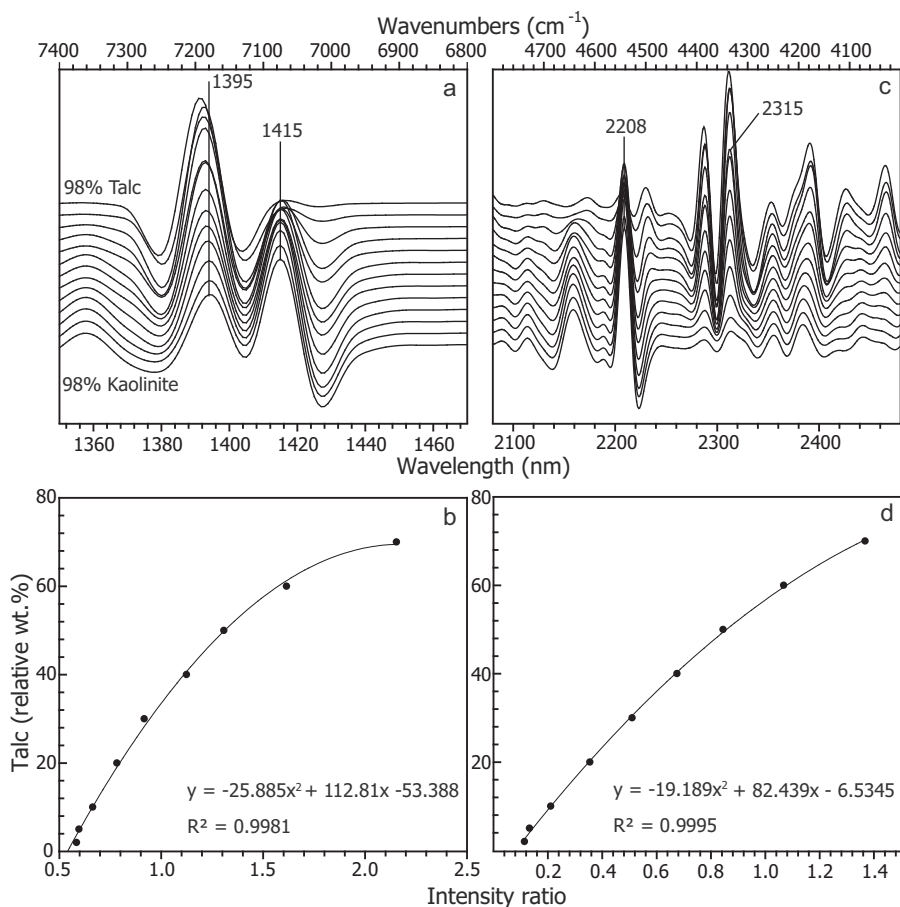
Fig. 10. Second derivative spectra (a and c) and calibration curves (b and d) of the talc-kaolinite binary admixture series. Reflectance spectra were acquired with the field spectrometer and derived using TSG.

evolution due to phyllosilicate content variation.

The intensity ratio can be negative because we also chose to consider the negative intensity values of the muscovite component that occur at 2195 nm. The correlation between the qualitative parameter and the muscovite content is validated for muscovite percentages ranging between 2 and 70 wt%. This correlation permits the detection of muscovite once its percentage reaches 5 wt% in the clay mixture.

The 2360 nm component shifted to 2350 nm while moving from the kaolinite-rich to the muscovite-rich mixtures. The intensity of the 2350 nm component remained constant, while the intensity of the component at 2385 nm decreased. A second qualitative parameter was defined as I_{2350}/I_{2385}. A correlation (Fig. 9d) was observed for mixtures containing percentages of muscovite ranging from 2 to 70 wt%. This second qualitative parameter allows the detection of muscovite once its percentage reaches 10 wt%.

4.10. Kaolinite–talc mixtures

In the second ROI (Fig. 10a) the component at 1395 nm is due to both kaolinite and talc. A slight shift towards 1388 nm is observed when the relative amount of kaolinite increases. The qualitative parameter used for talc is I_{1395}/I_{1415} (Fig. 10b).

In the first ROI (Fig. 10c), kaolinite and talc showed several components. The 2315 nm and 2208 nm components were selected as representative of the contribution of talc and kaolinite, respectively. The qualitative parameter used for talc is the intensity ratio of both components, i.e., I_{2315}/I_{2208} (Fig. 10d). For both regions of interest

(1350–1470 nm and 2080–2480 nm), the limit of detection limit of talc mixed with kaolinite is 5 wt%.

4.11. Kaolinite–Fe-Mg chlorite mixtures

Within the second ROI (Fig. 11a) chlorite showed only a broad peak at approximately 1410 nm, which was partly overlapped by two peaks related to kaolinite (1395 and 1415 nm). The qualitative parameter was given by I_{1415}/I_{1395}. A good correlation between the relative content of chlorite, and the qualitative parameter has been observed for samples containing from 2 to 50 wt% chlorite (Fig. 11b). The detection limit of chlorite mixed with kaolinite is 5 wt%.

In the first ROI (Fig. 11c), chlorite is characterized by three components located at 2205, 2255 and 2350 nm. Kaolinite showed two main components at 2160 and 2208 nm, and a triplet was observed at 2320, 2355 and 2385 nm. Both chlorite and kaolinite have components near 2350 nm. However, a shift from 2355 to 2350 nm is observed with increasing chlorite content in the binary mixtures. The qualitative parameter used for chlorite is I_{2250}/I_{2355}. A good correlation has been observed between the proportion of chlorite, expressed as a percentage, in the mixture and its qualitative parameter (Fig. 11d). The detection limit of chlorite mixed with kaolinite is also 5 wt%.

4.12. Smectite–Fe-Mg chlorite mixtures

In the first ROI, the main components of smectite and chlorite are located at 2205 nm and 2255 nm respectively (Fig. 12a). The
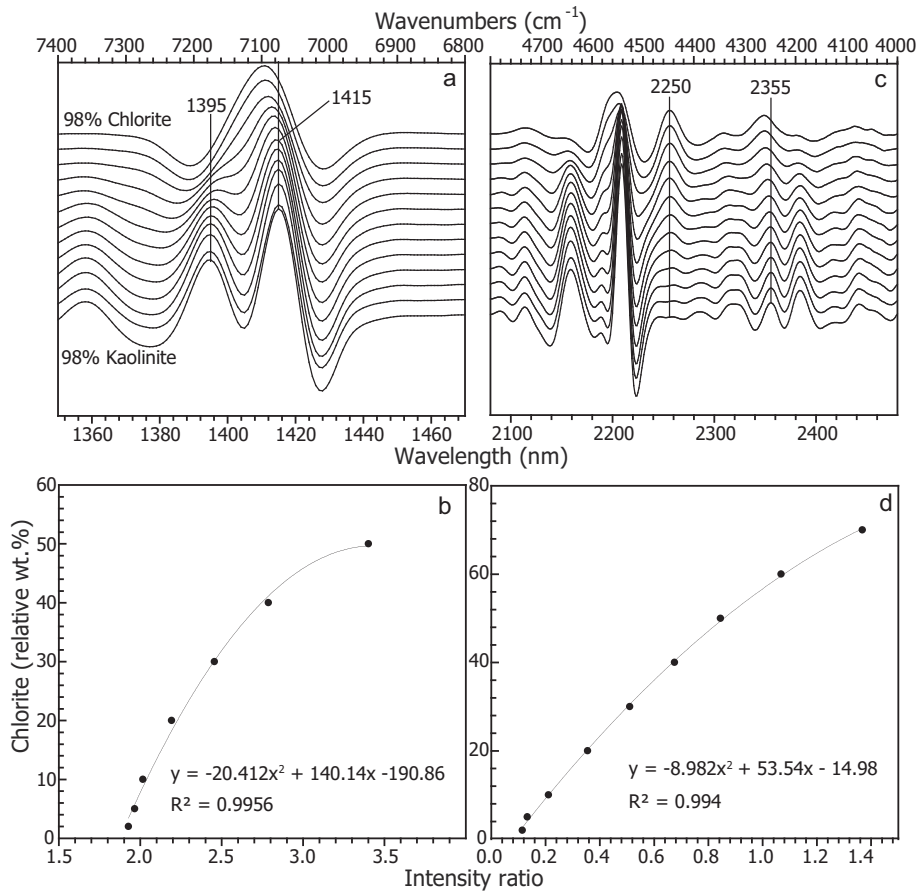
Fig. 11. Second derivative spectra (a and c) and calibration curves (b and d) of the chlorite-kaolinite binary admixture series. Reflectance spectra were acquired with the field spectrometer and derived using TSG.

qualitative parameter used for chlorite mixed with smectite is I_{2255}/I_{2205}. A good correlation is observed (Fig. 12b) between this qualitative parameter and the relative content of chlorite. The detection limit of chlorite mixed with smectite is 5 wt%. No significant changes in the profile of the secondary derivative spectrum are observed in the second ROI.

4.13. Smectite–clinochlore mixtures

Unlike the smectite-chlorite binary admixtures (Fig. 12a), a gradual change can be observed between two distinct components of the clinochlore/smectite series in the second ROI (Fig. 13a). These two components occurring at 1392 and 1415 nm correspond to clinochlore bands, however smectite also share this 1415 nm band. The qualitative parameter for clinochlore is I_{1392}/I_{1415}, and there is a good correlation with the percentage of clinochlore in the mixture (Fig. 13b).

In the first ROI (Fig. 13c), the two components at 2208 and 2238 nm were related to smectite. Clinochlore has two main components located at 2245 and 2290 nm and several broader components from 2300 to 2400 nm. The qualitative parameter for clinochlore is given by I_{2245}/I_{2208}. Fig. 13d showed a good correlation between the percentage of clinochlore and the intensity ratio I_{2245}/I_{2208}. The detection limit of clinochlore is equals to 10 wt% in both regions of interest.
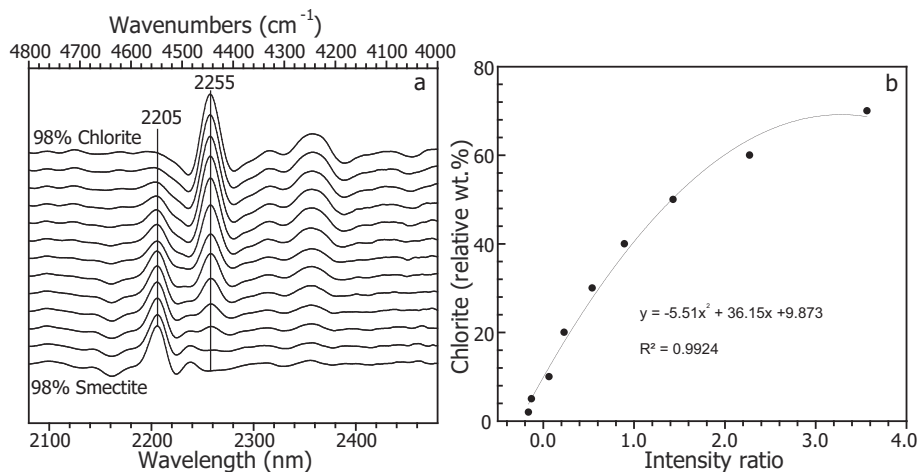

Fig. 12. Second derivative spectra (a) and calibration curve (b) of the chlorite-smectite binary admixture series. Reflectance spectra were acquired with the field spectrometer and derived using TSG.
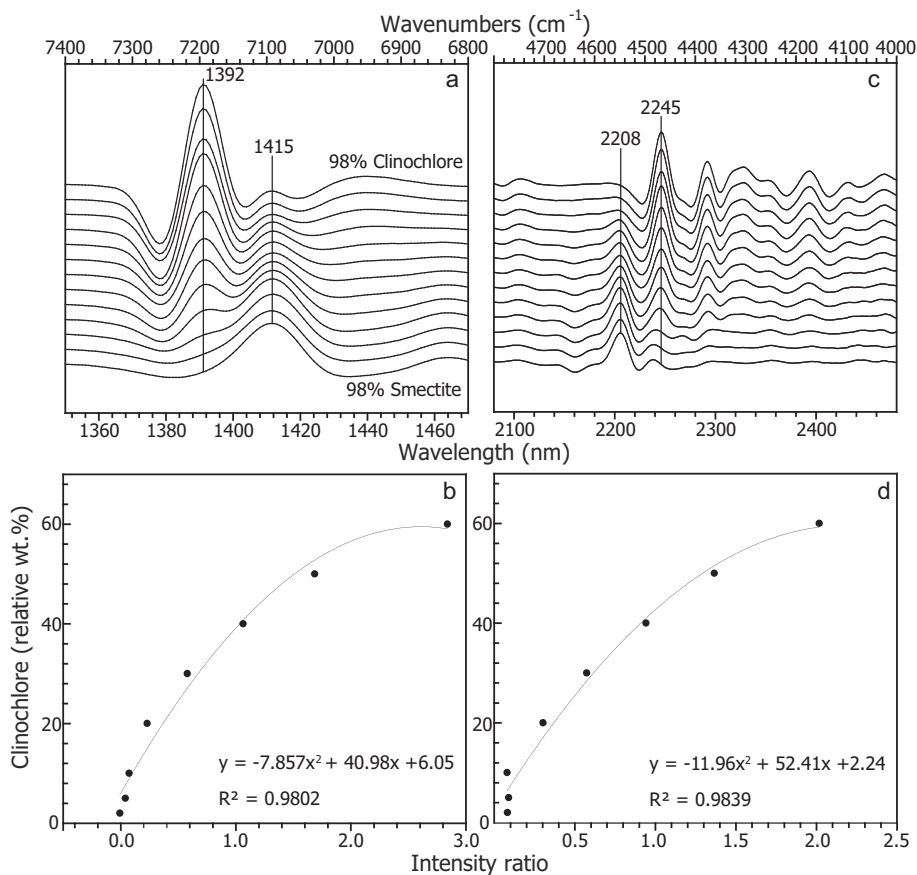
Fig. 13. Second derivative spectra (a and c) and calibration curves (b and d) of the clinochlore-smectite binary admixture series. Reflectance spectra were acquired with the field spectrometer and derived using TSG.

5. Application to natural samples

The complete procedure about how to use the second derivative methodology is described step by step in Appendix 7. The 8 samples selected for the application of this second derivative methodology showed weak (Ity 1, 9, 14 and 19) to very weak contributions (Ity 4, 7, 12 and 20) of hypogene phyllosilicates in the NIR spectra (Fig. 14). However, their presence was confirmed by XRD analysis of the fine-grained fraction of each sample. Four different phyllosilicate associations, previously described in the methodological sections of this paper, were observed: kaolinite – muscovite (Ity 1 and 12), smectite – Fe-Mg chlorite (Ity 19 and 20), smectite – clinochlore (Ity 9 and 4), and kaolinite – talc (Ity 14 and 7).

The resolution of the NIR spectra collected from these natural samples is lower than those collected for the binary mixtures. This is due to the difference in matrix composition that exists between experimental and natural samples, and more particularly to the presence of significant amount of inactive minerals (i.e. which do not absorb the IR radiation in the NIR domain) in the samples of saprolite (quartz, some silicates…).

For each mixture of clay minerals, qualitative parameters (Appendix 8) were calculated for both ROI using the methodology described in this paper. These qualitative parameters were compared to the values established as detection limits from calibration curves (Figs. 8 to 12). In samples where the qualitative parameter values from the NIR spectra were above the detection limit, an estimation of the relative proportions of phyllosilicates was performed using the corresponding calibration curves equations within each ROI (cf. the results section).

For Ity 19 and 20, containing Fe-Mg chlorite and Ity 9 and 4, containing clinochlore in a smectite-rich matrix, the use of the second ROI was not found relevant. Such samples seem to have very low relative content of chlorite. However, chlorite and clinochlore were much more easily detected using the first ROI qualitative parameters.

The use of the calibration curves formula of those parameters for both types of samples show that Ity 19 and 20 contain a chlorite relative content around 11 wt% and 13 wt% of the total phyllosilicate content. On the other hand, Ity 9 and 4, appeared to have a relative clinochlore content of 10 wt% and 15 wt%. Note that Ity 4 showed an intermediate NIR profile between those of the binary admixtures with relative clinochlore contents of 10 and 20 wt%. Ity 14 and 7, which contained talc in a kaolinite-rich matrix, yielded qualitative parameters that correspond to values below the detection limit. It cannot be certified that talc is present in these samples. This methodology was then correctly applied to Ity 1 and 12, where muscovite was identified. The estimation of its relative content using calibration curve equations was successful, giving about 65 and 15 wt% respectively.

For each sample, estimations of the main phyllosilicates percentages have been done using a procedure based on XRD results and normative calculations (Quirt, 1995). Those estimations were made considering only the presence of the major phyllosilicates present within the sample and not the minor phases. The given percentages can so be considered as the maximum amount of hypogene and supergene phyllosilicates included in each samples.

The results of those calculations are presented in the Table 1, it appears that the percentages of different types of hypogene phyllosilicates determined by NIR spectroscopy using the second derivative

a

b
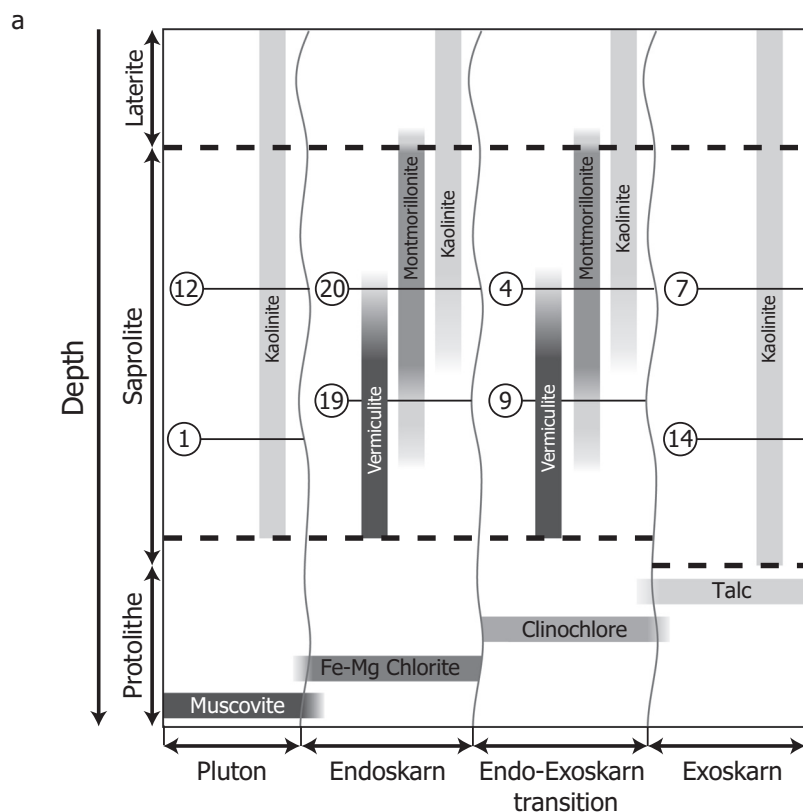
Fig. 14. Alteration zoning in the saprolite above the skarn deposit of Ity with specific phyllosilicate associations and location of the samples analyzed with NIR spectrometry using the second derivative method. Ity 1 and 12 are coming from unaltered pluton/volcano sediments and contain small amounts in muscovite. Ity 19 and 20 are coming from endoskarn and contain small amounts Fe-Mg chlorite. Ity 9 and 4 are coming from endo/exoskarn transition and contain small amounts of Mg chlorite (clinochlore). Ity 14 and 7 are coming from exoskarn and contain small amounts of talc. Note that no depth values are presented here because of the high variability of the laterite thickness (average of 10 m of depth) and of the saprolite (from 40 to 130 m).
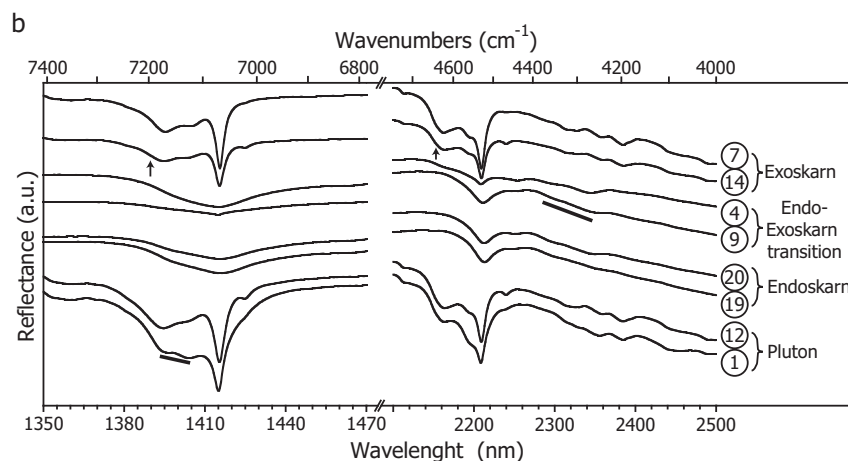
method are in agreement with the semi-quantitative estimations obtained from XRD and normative calculation. A variation up to < 15% is visible between both semi-quantitative estimations, probably due to the choice made during the normative calculations and the crystal-chemistry changes between the natural phyllosilicate and the one used to make the calibration curves. Indeed, substitutions and structural defects will have an influence on the IR bands and will so affect the second derivative components intensity.

The second derivative method was successfully applied to 8 samples from the Ity gold mine. It shown that it can be efficiently applied to natural samples to determine the nature of hypogene phyllosilicates disseminated in a lateritic saprolite, as well as providing semi-quantitative information about their relative abundance, which could be of interest for further mapping of the alteration at a regional scale.

6. Concluding remarks

Most of the major worldwide mining companies presently use field-based near-infrared spectroscopy for prospecting of ore deposits and acquiring in-depth knowledge of their associated alteration systems (Hauff, 2014). In addition to simple and instantaneous mineral identification, this methodology has great potential for the relative amounts of alteration minerals determination. It hence to map at field scales the alteration mineralogy zoning, which is often quite diagnostic of the proximity to ore. However, the utilization of field-based reflectance spectroscopy for qualitative and semi-qualitative investigations of phyllosilicates still requires improvement. In particular, care must be taken in the basic interpretation of the absorption features of the reflectance spectra if comparisons are only made with spectral data from

Table 1

Table with the main minerals contained in the 8 natural samples studied with the second derivative methodology. Their total contents in the different oxides used for the normative calculations are presented as well as the results of those calculations. For those semi-quantitative calculations the K_2O/Al_2O_3 ratio considered for the muscovite is equal to 3,18, the K_2O percentage for muscovite used is equal to 11%. It has been considered that clinochlore is containing 33% of MgO and 22% of Al_2O_3 and talc 30% of MgO. The Fe-Mg chlorite is containing 19% of MgO and 20% of Al_2O_3. Those values are average current percentage values for those kinds of phyllosilicates. The hypogene phyllosilicate percentages given in this table are considered as the maximum percentage of those minerals. Indeed, some minor phases, such as tremolite for example, can be present in few percent in each sample and have not been considered in those calculations.

Sample name	Main phyllosilicates	SiO_2 (%)	Al_2O_3 (%)	Fe_2O_3 (%)	MgO (%)	K_2O (%)	% hypogene phyllosilicate	% supergene phyllosilicate	Ratio hypogene phyllosilicate (%)	IR ratio hypogene phyllosilicate (%)
Ity 1	Kaolinite, muscovite	76.03	14.39	0.88	0.22	2.68	24%	15%	61%	65%
Ity 12	Kaolinite, muscovite	60.05	21.45	6.07	0.14	0.33	3%	54%	5%	15%
Ity 19	Smectite, Fe-Mg chlorite	53.85	13.99	5.89	5.85	0.63	4%	66%	6%	11%
Ity 20	Smectite, Fe-Mg chlorite	46.6	15.39	8.42	8.68	1.46	21%	56%	27%	13%
Ity 9	Smectite, clinochlore	50.82	14.13	7.24	7.74	0.61	12%	58%	17%	10%
Ity 4	Smectite, clinochlore	48.38	15.66	8.1	2.9	0.48	9%	69%	11%	15%
Ity 14	Kaolinite, talc	38.1	28.68	16.44	0.07	0.04	0.002%	75%	< 1%	Under limit
Ity 7	Kaolinite, talc	36.46	31.67	14.36	0.2	0.05	0.006%	83%	< 1%	Under limit

Table 2

Table summarising the visual and second derivative detection limits of hypogene phyllosilicates in kaolinite or smectite-rich sample, in both regions of interest, for both field and laboratory spectrometer. Percentages are weight percentages.

Supergene phyllosilicate	Hypogene phyllosilicate	Laboratory NIR spectrometer				Field NIR spectrometer			
		Reflectance 1st ROI	2nd derivative 1st ROI	Reflectance 2nd ROI	2nd derivative 2nd ROI	Reflectance 1st ROI	2nd derivative 1st ROI	Reflectance 2nd ROI	2nd derivative 2nd ROI
Kaolinite	Talc	10%	5%	10%	5%	10%	5%	10%	5%
Kaolinite	Muscovite	40%	20%	40%	40%	50%	5%/10%	40%	–
Kaolinite	Fe-Mg chlorite	40%	5%	40%	–	40%	5%	30%	5%
Montmorillonite	Fe-Mg chlorite	30%	10%	50%	–	20%	5%	40%	–
Montmorillonite	Clinochlore	30%	5%	20%	5%	30%	10%	30%	10%

a routine library. The absorption bands of an unknown/uncharacterized clay mineral species are impacted by of several parameters (crystal chemistry, the degree of crystallinity, texture, water content, concentration, and matrix composition, as well as other factors), which cannot be addressed through the use of reference spectra chosen by an algorithm.

The main goal of this methodological study was to improve the use of field-based Near-IR spectroscopy for the detailed investigation of the phyllosilicates related to hypogene ore deposits at depth, based on overlying kaolinized saprolite. Saprolite is well known as the worst material in which to identify the distinctive spectral signatures of hypogene phyllosilicates such as muscovite-illite, chlorite or talc. Indeed, they are largely obliterated by the absorption features of kaolinite and/ or smectite that predominate in alteration profiles. However, properly determining the mineralogical composition and the spatial distribution of hypogene alteration products using reflectance spectroscopy in saprolite would significantly reduce the expenditure on exploration for metal deposits located in intertropical countries.

This study showed that it is possible to lower the detection limits of hypogene phyllosilicates to < 10% of the clay material of the saprolites (Table 2), provided that we use the second derivative methodology. The application of such a methodological procedure can also provide semi-quantitative estimation of hypogene phyllosilicates in lateritic clays. These two variables constitute an important prerequisite to the mapping of the alteration zoning of ore deposits at depth that are located under lateritic covers.

Using the NIR spectroscopy, it is important to keep in mind that the accuracy of identification and semi-quantification of phyllosilicates will be substantially improved if the unknown spectra are compared with those of mixtures made of standards phyllosilicates which crystal characteristics are similar to those of the phyllosilicates of the studied exploration area. Indeed as explain earlier, crystal-chemistry of those minerals will influence their second derivative spectra and will probably cause slight changes on the calibration curve. Choosing appropriate mineral references and calibration curves would minimize the influence of unaddressed variables, such as crystal chemistry and the degree of crystallinity, on the position and the profile of the infrared bands of natural or synthetic phyllosilicates (Hunt, 1977; Hauff, 2014; Aung et al., 2015). The impact of those changes must be tested in order to enhance this methodology.

Only binary admixtures of phyllosilicates have been tested to produce the calibration curves. However, new calibration curves must be established if more than two major types of phyllosilicates coexist in the studied natural samples. Note that the semi-quantitative estimation of phyllosilicates ratio obtained from the calibration curves are relevant even if they seem less accurate compared to the results of other longer quantification methodologies.
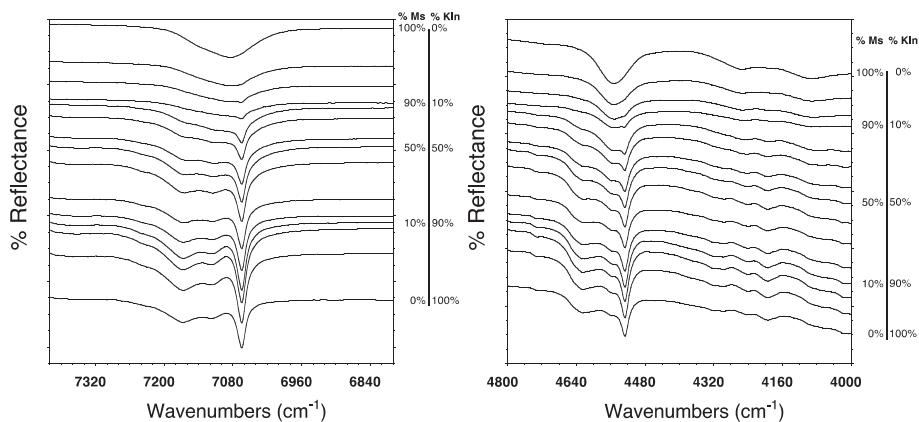
Appendix

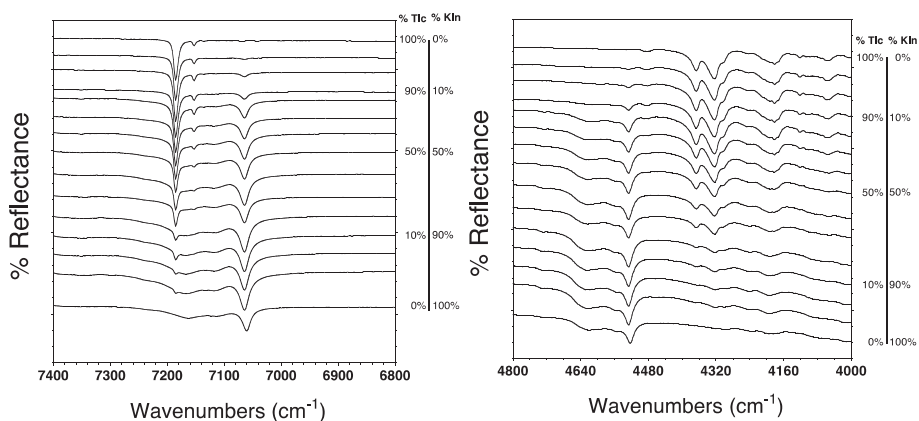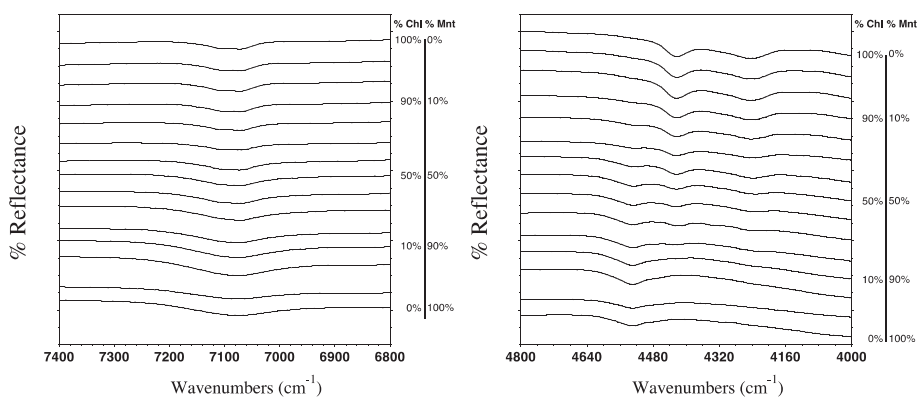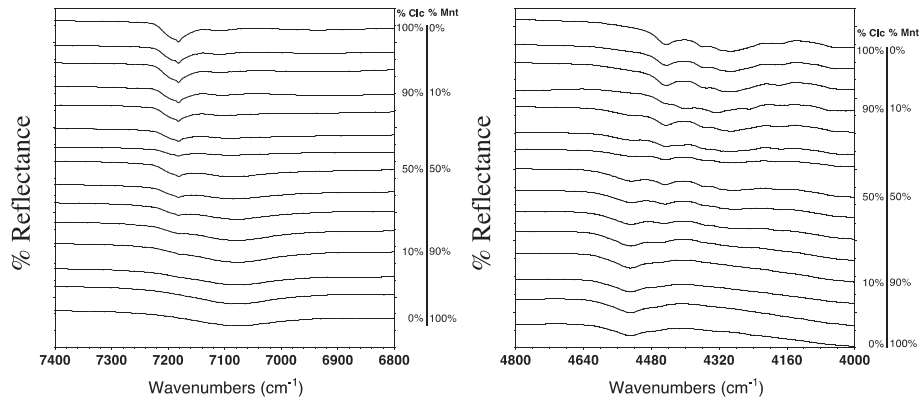**Appendix 1.** Binary mixtures spectral evolution of the kaolinite-muscovite series. The IR spectra (% Kln/% Ms) are corresponding from bottom to the top to 100/0; 98/2; 95/5; 90/10; 80/20; 70/30; 60/40; 50/50; 40/60; 30/70; 20/80; 10/90; 5/95; 2/98; 0/100 in the first (A) and second ROI (B).

Appendix 2. Binary mixtures spectral evolution of the kaolinite-talc series. The IR spectra (% Kln/% Tlc) are corresponding from bottom to the top to 100/0; 98/2; 95/5; 90/10; 80/20; 70/30; 60/40; 50/50; 40/60; 30/70; 20/80; 10/90; 5/95; 2/98; 0/100 in the first (A) and second ROI (B)

Appendix 3. Binary mixtures spectral evolution of the montmorillonite-Fe-Mg chlorite series. The IR spectra (% Mnt/% Chl) are corresponding from bottom to the top to 100/0; 98/2; 95/5; 90/10; 80/20; 70/30; 60/40; 50/50; 40/60; 30/70; 20/80; 10/90; 5/95; 2/98; 0/100 in the first (A) and second ROI (B)

Appendix 4. Binary mixtures spectral evolution of the montmorillonite-clinochlore series. The IR spectra (% Mnt/% Clc) are corresponding from bottom to the top to 100/0; 98/2; 95/5; 90/10; 80/20; 70/30; 60/40; 50/50; 40/60; 30/70; 20/80; 10/90; 5/95; 2/98; 0/100 in the first (A) and second ROI (B)
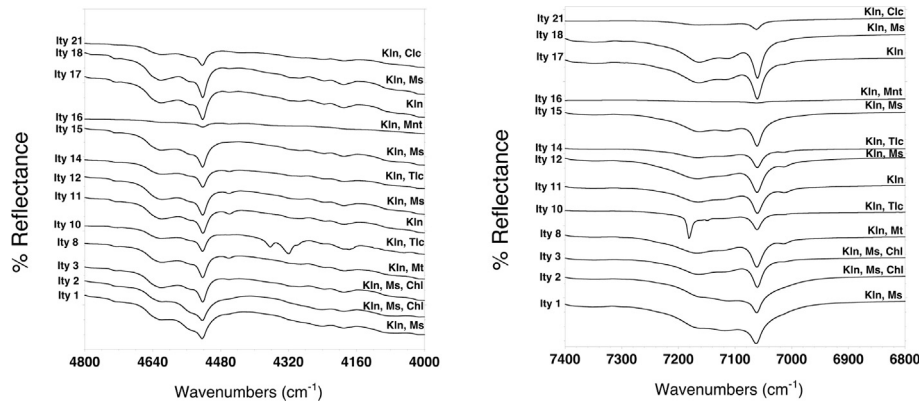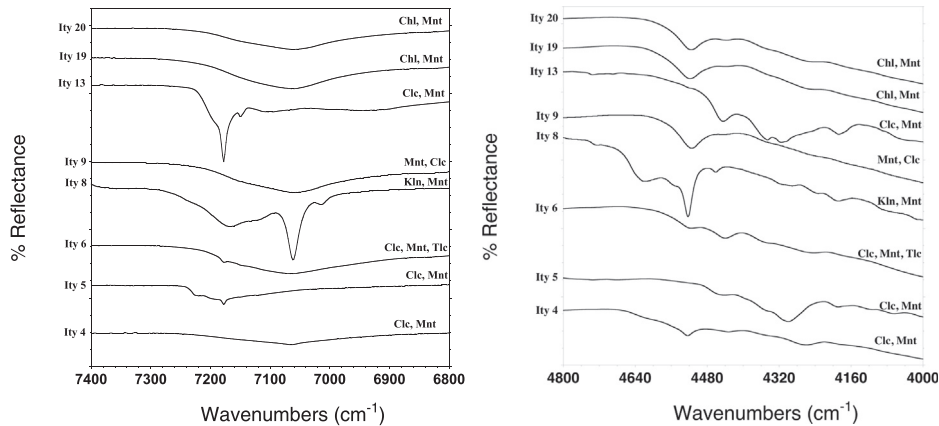

Appendix 5. IR spectra of the Ity kaolinite-rich samples and their corresponding mineralogy in the first and second ROI. Only the major phyllosilicates phases are described here, others like montmorillonite, talc and chlorite can also be present in the samples but under the detection limit of the IR

Appendix 6. IR spectra of the Ity montmorillonite-rich samples and their corresponding mineralogy in the first and second ROI. Only the major phyllosilicates phases are described there, others like talc and kaolinite can also be present in the samples but under the detection limit of the IR

Appendix 7. So how to use the second derivative methodology ?

1- After collecting samples in the field, crush them slightly to obtain a homogeneous powder. Crushing under ethanol prevents any crystallographic disturbance.

2- Dry the sample powders to prevent water disturbance of the IR signal. It can be done using a microwave oven for quicker drying (as described in the Sampling section).

3- Acquire the IR spectra of the sample powders with a field-based spectrometer.

4- From this step, you must be able to recognize the supergene phyllosilicate and/or the hypogene phyllosilicate IR diagnostic bands using the absorption band wavelengths provided in the first part of this work. In case where hypogene IR bands are clearly visible on the spectra, there is no need to use the second derivative methodology. In the other case you will need to apply this very sensitive methodology.

5- In case you suppose the presence of hypogene or supergene phyllosilicates but you are not seeing them clearly, apply the derivation process on your samples spectra using the software related to the spectrometer. Remember, there is no second derivative option for The Spectral Geologist™ (TSG) software, you can directly use this option without further steps. If you use the OMNIC™ software, we advise you to choose "a set of 13 points" parameter and a "polynomial function of order 3" to get the optimal second derivative spectrum resolution.

6- Select the intensity ratios that correspond to the combination of the main hypogene and supergene phyllosilicates of your samples individually (Appendix 8).

7- Measure the intensity values, from the second derivative curve (from Y = 0 to your maximal/minimal intensity), at the two specified wavelengths of the intensity ratio that you selected. Calculate the ratio value and use it in the regression curve formula to see if the target phyllosilicate is present or not. You can also obtain the relative percentage of the target phyllosilicate compared to the total mass of phyllosilicate of your sample.

In case where the relative percentage value would be lower than the detection limit established in this work (Table 2), this methodology cannot assess that the target phyllosilicate is present in the sample.

In case where the relative percentage value would be higher than the detection limit, this value can be considered as an imprecise semi-quantitative value, in the range defined by the calibration curve.

You can also compare the estimated relative percentage obtained from the first and second ROI (if available).

Appendix 8
Table with the qualitative parameters of each binary admixture and the related detection limits for both ROI

Binary admixture	1st ROI qualitative parameter	Detection limit	2nd ROI qualitative parameter	Detection limit
Kaolinite/muscovite	I_{2195}/I_{2208}	5%	I_{1395}/I_{1415}	70%
	I_{2350}/I_{2385}	10%		
Kaolinite/talc	I_{2315}/I_{2208}	5%	I_{1395}/I_{1415}	5%
Kaolinite/chlorite	I_{2250}/I_{2355}	5%	I_{1415}/I_{1395}	5%
Smectite/chlorite	I_{2255}/I_{2205}	5%	/	/
Smectite/clinochlore	I_{2245}/I_{2208}	10%	I_{1392}/I_{1415}	10%

References

Aung, L.L., Tertre, E., Petit, S., 2015. Effect of the morphology of synthetic kaolinites on their sorption properties. J. Colloid Interface Sci. 443, 177–186.

Baron, F., Petit, S., 2016. Interpretation of the infrared spectra of the lizardite-nepouite series in the near- and mid-infrared range. Am. Mineral. 101, 423–430.

Béziat, D., Siebenaller, L., Salvi, S., Chevalier, P., 2016. A weathered skarn-type mineralization in Ivory Coast: the Ity gold deposit. Ore Geol. Rev. 78, 724–730.

Bishop, J.L., Lane, M.D., Dyar, M.D., Brown, A.J., 2008. Reflectance and emission spectroscopy study of four groups of phyllosilicates: smectites, kaolinite-serpentines, chlorites and micas. Clay Miner. 43, 35–54.

Cerny, P., Blevin, P.L., Cuney, M., London, D., 2005. Granite-related ore deposits. In: Economic Geology, 100th Anniversary Volume, pp. 337–370.

Dalm, M., Buxton, M.W.N., Van Ruitenbeek, F.J.A., Voncken, J.H.L., 2017. Application of near-infrared spectroscopy to sensor based sorting of a porphyry copper ore. Miner. Eng. 58, 7–16.

Dill, H.G., 2016. Kaolin: Soil, rock and ore from the mineral to the magmatic, sedimentary and metamorphic environment. Earth-Sci. Rev. 161, 16–129.

Edwards, R.P., Atkinsons, K., 1986. Ore Deposit Geology and Its Influence on Mineral Exploration. Springer, Netherland.

Einaudi, M.T., 1982. General features and origin of skarns associated with porphyry copper. In: Advances in Geology of the Porphyry Copper Deposits Southwestern North America. The University of Arizona Press, Tucson (Arizona), pp. 185–210.

Ferrage, E., Martin, F., Micoud, P., Petit, S., Parseval, P., Beziat, D., Ferret, J., 2003. Cation site distribution in clinochlores a NIR approach. Clay Miner. 38, 329–338.

Feybesse, J.L., Milési, J.P., 1994. The Archean/Proterozoic contact zone in West Africa: a mountain belt of décollement thrusting and folding on a continental margin related to 2.1 Ga convergence of Archaean craton? Precambrian Res. 69, 199–227.

Hauff, P., 2014. An Overview of VIS-NIR-SWIR Field Spectroscopy as Applied to Precious Metals Exploration. Spectral International Inc.

Herrmann, W., Blake, M., Doyle, M., Huston, D., Kamprad, J., Merry, N., Pontual, S., 2001. Short wavelength infrared (SWIR) spectral analysis of hydrothermal alteration zones associated with base metal sulphide deposits at Roseberv and Western Tharsis, Tasmania, and Highway Reward, Queensland. Econ. Geol. 96 (5), 939–955.

Hirdes, W., Davis, D.W., Lüdtke, G., Konan, G., 1996. Two generation of Birimian (Paleoproterozoic) volcanic belts in northeastern Côte d'Ivoire (West Africa): consequences for the Birimian controversy. Precambrian Res. 80, 173–191.

Hunt, G.R., 1977. Spectral signatures of particulate minerals in the visible and near infrared. Geophysics 42, 501–513.

Hunt, G.R., Ashley, R.P., 1979. Spectra of altered rocks in the visible and near infrared. Econ. Geol. 74 (7), 1613–1629.

Joussein, E., Petit, S., Decarreau, A., 2001. Une nouvelle méthode de dosage des minéraux argileux en mélange par spectroscopie IR. C. R. Acad. Sci. Ser. IIA, Earth Planet. Sci. 332, 83–89.

Lawrence, D.M., Treolar, P.J., Rankin, A.H., Harbidge, P., Holliday, J., 2013a. The geology and mineralogy of the Loulo mining district, Mali, West Africa: evidence for two distinct styles of orogenic gold mineralization. Econ. Geol. 108, 199–227.

Lawrence, D.M., Treolar, P.J., Rankin, A.H., Boyce, A., Harbidge, P., 2013b. A fluid inclusion and stable isotopes study at the Loulo mining district, Mali, West Africa: implication for multifluid sources in the generation of orogenic gold deposits. Econ. Geol. 108, 229–257.

Leube, A., Hirdes, W., Mauer, R., Kesse, G.O., 1990. The early Proterozoic Birimian supergroup of Ghana and some aspects of its associated gold mineralization. Precambrian Res. 46, 139–165.

Lisowiec, N., Halley, S., H., Ryan, L., 2007. Using deposit-scale alteration and geochemical signatures to explore for analogue deposits: a case study from the Mt Wright Gold Project, Queensland. In: Geochemical Case Histories and Geochemical Exploration Methods, pp. 969–972.

Madejova, J., Balan, E., Petit, S., 2011. Application of vibrational spectroscopy to the characterization of pylloslicates and other industrial minerals. In: EMU Notes in Mineralogy. vol. 9. European Mineralogical Union, pp. 171–226.

Mathian, M., Beaufort, D., Lescuyer, J.L., Furic, R., 2015. Application de la spectroscopie infrarouge portable à l'identification des phyllosilicates des roches sous couverture latéritique: Cas d'étude du prospect minier du Mont Ity (Côte d'Ivoire) (Master thesis). .

Meinert, L., Dipple, G.M., Nicolescu, S., 2005. World skarn deposits. In: Economic Geology, 100th Anniversary Volume, pp. 299–336.

Milesi, J.P., Feybesse, J.L., Ledru, P., Domanget, A., Ouedraogo, M.F., Marcoux, É., Prost, A., Vinchon, C., Sylvain, J.P., Johan, V., Tegyey, M., Calvez, J.Y., Lagny, P., 1989. Les minéralisations aurifères de l'Afrique de l'Ouest. Chron. Rech. Min. 497, 3–98.

Petit, S., Madejova, J., Decarreau, A., Martin, F., 1999. Characterization of octahedral substitutions in kaolinites using near infrared spectroscopy. Clay Clay Miner. 47, 103–108.

Petit, S., Decarreau, A., Martin, F., Buchet, R., 2004a. Refined relationship between the position of the fundamental OH stretching and the first overtones for clays. Phys. Chem. Miner. 31, 585–592.

Petit, S., Martin, F., Wiewiora, A., De Parseval, P., Decarreau, A., 2004b. Crystal-chemistry of talc: a near infrared (NIR) spectroscopy study. Am. Mineral. 89, 319–326.

Pontual, S., Merry, N., Gamson, P., 1997. Spectral Interpretation Field Manual GMEX. AusSpec International Pty.

Post, J.L., Crawford, S.M., 2014. Use of near-infrared spectra for the identification of clay minerals. Appl. Clay Sci. 95, 383–387.

Post, J.L., Noble, P.N., 1993. The near-infrared combination band frequencies of

dioctahedral smectites, micas and illites. Clay Clay Miner. 41 (6), 639–644.

Quirt, D.H., 1995. Norm calculation procedure for sandstone clay minerals. In: Saskatchewan Research Council, Publication No. R-1230-28-E-95, pp. 14.

Ramanaidou, E.R., Wells, M., 2015. A new toolkit for iron ore characterisation. Proc. Iron Ore 2015, 587–590.

Seedorff, E., Dilles, J.H., Proffett Jr., J.M., Einaudi, M.T., Zurcher, L., Stavast, W.J.A., Johnson, D.A., Barton, M.D., 2005. Porphyry deposits: characteristics and origin of hypogene features. In: Economic Geology, 100th Anniversary Volume, pp. 251–298.

Simmons, S.F., White, N.C., John, D., 2005. Geological characteristics of epithermal precious and base metal deposits. In: Economic Geology, 100th Anniversary Volume, pp. 485–522.

Sun, Y., Seccombe, P.K., Yang, K., 2001. Application of short-wave infrared spectroscopy to define alteration zones associated with the Elura zinc-lead-silver deposit, NSW, Australia. J. Geochem. Explor. 73, 11–26.

Thompson, A.J.B., Hauff, P.L., Robitaille, A.J., 1999. Alteration mapping in exploration: application of short-wave infrared (SWIR) spectroscopy. Soc. Econ. Geol., Newsl. 39, 16–27.

Vaculikova, L., Plevova, E., 2005. Identification of clay minerals and micas in sedimentary rocks. Acta Geodyn. Geomater. 2 (138), 167–175.